Note: This is the last version of manuscript prior to acceptance. There are only minor changes between this and the published article.

Zhang G, Nan Z, Yin Z, Zhao L. Isolating the contributions of seasonal climate warming to permafrost thermal responses over the Qinghai - Tibet Plateau. Journal of Geophysical Research: Atmospheres. 2021, 126(e2021JD035218). doi:10.1029/2021JD035218.

Isolating the contributions of seasonal climate warming to permafrost thermal responses over the Qinghai-Tibet Plateau

Guofei Zhang[1], Zhuotong Nan[*1, 2], Ziyun Yin[1], Lin Zhao[3]

[1]Key Laboratory of Ministry of Education on Virtual Geographic Environment, Nanjing Normal University, Nanjing 210023, China. [2]Jiangsu Center for Collaborative Innovation in Geographical Information Resource Development and Application, Nanjing 210023, China. [3]School of Geographical Sciences, Nanjing University of Information Science & Technology, Nanjing 210044, China.

[*]Correspondence to: Zhuotong Nan, e-mail: nanzt@njnu.edu.cn

Key Points

- Contributions of seasonal warming to permafrost thermal responses are isolated by specially designed numerical scenarios based on historical records
- Permafrost in the Three River Source region and the Qiangtang High Plateau is vulnerable to thermal degradation induced by winter warming
- One-degree air temperature warming in summer lead to an increase of 0.35 m in ALT and of 0.20 °C in MAGT, while in winter, an increase of 0.16 m and 0.13 °C, respectively

Abstract

Climate warming is thermally degrading permafrost. The climate warming over the Qinghai-Tibet Plateau (QTP) is characterized by obvious seasonality and stronger winter warming in comparison with summer warming in 2000s. The contributions of seasonal climate warming to permafrost thermal responses remain unknown. Here we isolated the seasonal warming contributions to permafrost thermal regimes through contrasting a series of specially designed numerical experiments that were composed of decadal seasonal data segments. The results reveal that permafrost thermal regime is highly sensitive to winter temperature change. Permafrost in the Three River Source region and on the Qiangtang High Plateau has undergone remarkable thermal degradation in the 2000s due to winter warming. It was estimated that each degree of rising in air temperature in summer could lead to an average increase of 0.35 m in the active layer thickness (ALT) and of 0.20 °C in the mean annual ground temperature (MAGT), while for one-degree winter warming, the active layer thickens by 0.16 m and the MAGT increases by 0.13 °C. However, the overall impacts of winter warming have exceeded summer warming in 2000s due to a triple warming rate in winter than that in summer in this period.

Plain Language Summary

Known as the Earth's Third Pole, the Qinghai-Tibet Plateau (QTP) is the largest high-elevational permafrost zone in the world. Permafrost is a sensitive indicator for climate change and particularly sensitive to rising air temperature. The climate warming on the QTP is two times faster than the global average during last few decades and in recent decades, climate warming in winter has become larger than that in summer. Therefore, how permafrost responds to seasonal warming and how to distinguish the warming effects from the summer (May–October) and winter (November–April) worth investigating. Here we developed hypothetical numerical experiments and contrasted them with a baseline scenario for representing the historical air temperature conditions to isolate the respective contributions of seasonal climate warming. Six experiments were constructed by modifying the historical data where decadal summer or winter temperatures are held invariable throughout the whole time periods. We contrasted the simulated responses of permafrost over the QTP to winter and summer warming, and quantified the contributions to permafrost thermal regime per unit degree of winter and summer warming. This study provides insight into the permafrost responses to seasonal climate warming in the context of global warming.

Keywords: seasonal climate warming, quantitative contribution, permafrost, thermal regime, scenario analyses, Qinghai-Tibet Plateau

1. Introduction

The Qinghai-Tibet Plateau (QTP), the highest plateau in the world with an average elevation of over 4000 m above sea level (a.s.l.), is characterized by unique topography and geographical location. It is thus known as the “Third Pole”. Its thermal and dynamic effects exert profound influence on the regional climate and even the global climate system (*Yanai et al.*, 1992; *Duan and Wu*, 2005). Many important Asian rivers originate from the QTP, including the Yangtze River, the Yellow River and the Mekong River. It holds the largest ice storage after the polar regions, dubbed as the “Asian Water Tower”. It drains a lot of water to rivers and is particularly crucial for water resources on the Asian continent (*Xu et al.*, 2008; *Immerzeel et al.*, 2010; *Yao et al.*, 2019). The QTP covers an area of approximately 2.6×10^6 km^2, half of which is underlain by permafrost and accounts for 75% of alpine permafrost in the Northern Hemisphere (*Jin et al.*, 2000).

Permafrost is a product of long-term energy exchange between the atmosphere and the ground. It refers to the ground that remains at or below 0 °C for at least two consecutive years. Its existence and properties depend on regional climate and topography. Global warming has caused extensive permafrost degradation (*Smith et al.*, 2005; *Pepin et al.*, 2015; *Chadburn et al.*, 2017). The atmospheric circulations over the QTP are primarily influenced by the interaction between Indian monsoon, westerlies and East Asian monsoon (*Chen et al.*, 2008; *Molnar et al.*, 2010; *Yao et al.*, 2012; *Chiang et al.*, 2015). The climate on the QTP is thus highly sensitive to global climate change. It has been regarded as an early warning signal of global warming (*Pan and Li*, 1996; *Liu and Zhang*, 1998). Meteorological

observations show that the warming rate was 0.3–0.4 °C/decade (*Zhong et al.,* 2011; *Chen et al.,* 2015; *Yao et al.,* 2019), twice of the averages of globe and the Northern Hemisphere. Its warming rate has accelerated significantly since the 1980s (*You et al.,* 2010; *Wu et al.,* 2013; *Kuang and Jiao,* 2016). New thermokarst and thawing permafrost has been observed, resulting in numerous environmental, climatic and engineering problems, such as lowered groundwater table, undiversified species, accelerated land desertification, increased carbon release stored in frozen soils, and destabilization of human infrastructure (*Cheng and Wu,* 2007; *Li et al.,* 2008; *Kang et al.,* 2010; *Guo et al.,* 2012; *Cheng et al.,* 2019).

Despite overall climate warming over the QTP, the magnitudes of warming in seasons were different. The warming rate in winter was found to be greater than that in summer on the QTP (*Liu et al.,* 2009; *Wu et al.,* 2013; *You et al.,* 2013; *Duan et al.,* 2015). The increase rate of winter temperature on the QTP exceeded any areas at the same latitude in the Northern Hemisphere (*Liu and Chen,* 2000). The winter warming was projected by more than 3 °C (100% probability) for the period 2070–2099, which was much higher than summer warming (*Chen et al.,* 2011; *Rangwala et al.,* 2013; *Zhang et al.,* 2015). Currently, the prominent winter warming on the QTP has attracted wide attention (*Duan et al.,* 2015; *Duan and Xiao,* 2015; *Ma et al.,* 2019). Some observation-based study suggest that winter warming may lead to extensive permafrost degradation (*Wang et al.,* 2000). However, the observational evidences are inadequate due to a very limited number of observation sites distributed on the QTP. It becomes increasingly concerned how and in what extent permafrost responds to seasonal climate warming on the QTP. Hence, it is imperative to

understand the effects and different contributions of seasonal warming to permafrost dynamics, especially in the context of global warming.

To date, few studies has been conducted to investigate the responses of permafrost to seasonal climate warming. A potential obstacle is that the complex nature of freeze-thaw cycle in permafrost is hard to interpret by field measurements or remote sensing approaches. Numerical simulation is proven effective for understanding permafrost changes. It can explain the complex freeze-thaw cycles in physical terms and simulate permafrost changes on regional scales. In reality, changes in a single freeze-thaw cycle are always the combined results of seasonal variations of air temperature over a year. It is hard to isolate the impact of single season on permafrost dynamics. Our recent study proposed a numeric approach in attempt to revealing the potential impacts of seasonal climate warming on permafrost changes (*Zhang et al.*, 2019). Based on the Noah land surface model (LSM), two control experiments were conducted to identify individual effects of winter and summer warming on permafrost over the QTP. In its design, the winter scenario for testing the impacts of winter warming was composed by replacing all summer temperatures through the entire period with the first year's summer temperatures while retaining the historical winter temperatures. However, this method is inadequate in representing real seasonal warming conditions where warming in one season always comes together with the changes in the other seasons. As a result, it is most likely to bias the potential impact of winter warming on permafrost. More importantly, due to the methodological flaw in the previous study, it fails to provide

quantitative answers to the questions, such as how much permafrost degradation was induced in response to each degree of summer or winter warming.

In the present work, we have conceived numerical experiments that aim to quantify the respective contributions of seasonal climate warming to permafrost thermal responses. Instead of using totally hypothetical scenarios, we combined decadal seasonal data segments to make up the experimental scenarios so as to mimic the real warming trends as well as possible. Seasonal climate warming scenarios were constructed on the basis of the historical records by holding decadal summer (May–October) or winter (November–April) temperatures invariable through the entire study period, thereby representing distinct seasonal warming levels. Then, we comprehensively evaluated permafrost responses to winter and summer warming through a means of inter-comparison between the results from six hypothetical scenarios and the baseline scenario. At last, we isolated the contributions of winter and summer warming as the changes in permafrost indicators in response to one degree of seasonal climate warming.

2. Scenarios and Methodology

The model used in this study is the modified version of Noah LSM 3.4.1 (*Wu et al.*, 2018). It has been strengthened for modeling the permafrost dynamics and reflecting the environmental characteristics of the QTP. The main improvements include a modified thermal roughness scheme for sparse and dense vegetations and improved parameterization schemes of thermal and hydraulic conductivities to account for the prevalence of coarse-grained soils and the impedance of ground ice, as well as the extension of the

simulation depth to below 15m considering vertical soil heterogeneity. The model performance has been verified at a representative plateau permafrost site (*Wu et al.,* 2018). The details of the modeling procedure have been reported previously in *Zhang et al.* (2019).

Despite using a similar scenario-based numerical simulation approach, special designs and extra considerations were placed to enable isolating the contributions of seasonal climate warming to permafrost changes. The baseline scenario was based on the China Meteorological Forcing Dataset (CMFD) (*Chen et al.,* 2011). The CMFD includes seven atmospheric variables, i.e., air temperature, precipitation, wind speed, specific humidity, atmospheric pressure, downward solar radiation, and downward longwave radiation. The baseline aims to present the permafrost changes under historical climate conditions. To quantify the isolated contributions of seasonal climate warming, seasonal warming scenarios were constituted by intentionally modifying seasonal air temperature data in the baseline while retaining the other atmospheric variables. By contrasting the outcomes of these seasonal scenarios and the baseline, the individual impacts of seasonal warming were identified and quantified.

Studies have shown that the rising in air temperature is non-linear and varies in rate over periods (*Chen et al.,* 2015). An analysis of air temperature from 1980s to 2000s based on the CMFD shows a general increasing trend across the QTP but with distinct decadal magnitudes (black line in Figure 1a). The rates of temperature rise were 0.22, 0.89 and 0.98 °C/decade in the 1980s, 1990s, and 2000s, respectively. The last decade (the 2000s) had seen the highest warming rate. Meanwhile, different warming rates were observed in

summer and winter (Figure 1b). In the 1980s, seasonal variation in air temperature rise was relatively small, both at 0.22 °C/decade. However, interannual variability in changes of air temperatures over the QTP was accelerated in the continuously warming 1990s, with 0.80 °C/decade in winter and 0.98 °C/decade in summer. In the 2000s, the winter warming continued to accelerate whereas the summer warming slowed. The warming rates were 1.46 °C/decade in winter and 0.52 °C/decade in summer. Such seasonal variations were attributed to gross seasonal differences in atmospheric circulation (*Yao et al.*, 2012; *Kuang and Jiao*, 2016).

In wake of nonlinearity and seasonal distinctions in air temperature rising, we divided the entire study period into three stages, denoted by C1 for 1980–1989, C2 for 1990–1999 and C3 for 2000–2009, and each stage into winter (November–April) and summer (May–October) seasons. The division of seasonality primarily respects the distinctive characteristics of an annual freeze-thaw cycle (*Zhang et al.*, 2019). Accordingly, the historical air temperature data were segmented into multiple decadal winter and summer segments. The summer temperature time series in the baseline comprises of three segments: C1S, C2S and C3S for denoting summer temperature data in the 1980s, 1990s and 2000s, respectively. Likewise, winter temperature segments in the baseline are C1W, C2W and C3W for the respective three stages. C1S, C2S and C3S thus represent different levels of summer temperature variations that have already occurred, i.e., low (0.22 °C/decade), high (0.98 °C/decade), and medium (0.52 °C/decade), respectively. C1W, C2W and C3W represent different levels of winter temperature variations: low (0.22 °C/decade), medium (0.80 °C/decade), and high

(1.46 °C/decade). By fixing decade-wide seasonal temperatures to any of those segments, we constituted a variety of hypothetical seasonal scenarios, as listed in Table 1. SR1–SR3 represent summer scenarios with natural winter temperatures and hold decade-wide summer temperatures constant. They were created on the basis of the baseline by substituting summer temperatures throughout the entire period with the low (C1S), high (C2S) and medium (C3S) summer segments, respectively, while winter temperatures were held the same as the baseline. For instance, SR1 fixes the summer temperatures to a same C1S on behalf of relatively low summer temperature conditions in the 1980s. By such a design, long-term invariability and stage-wide variability in summer temperature can coexist within a scenario, so as to better represent real warming cases. The winter temperatures in SR1 are identical to those in the baseline. Similarly, SR4–SR6 represent various winter scenarios with natural summer temperatures and fixed winter temperatures. Their winter temperatures were fixed to the low (C1W), medium (C2W) and high (C3W) levels, respectively, while summer temperatures retain the baseline.

Table 1. Baseline and hypothetical scenarios by assembling decadal seasonal segments coming from the three decadal stages in the historic records.

In the hypothetical scenarios, there is no inter-stage change in temperature during a fixed season. By contrasting the simulation results of the hypothetical scenarios to the baseline, the effects of seasonal climate warming can be determined, because the hypothetical scenarios differ from the baseline only in air temperature of the fixed seasons without any differences in other atmospheric variables. In such way, impacts of any confounding variables such as

198 precipitation were excluded. Instead of using a single-year's seasonal air temperatures in the
199 replacement as adopted in *Zhang et al.* (2019), we maintained seasonal temperatures
200 constant between stages but allowed in-stage variabilities as a reflection of inherently
201 fluctuating nature of air temperature in a short period. This strategy is more consistent with
202 the actual situation than the one adopted in *Zhang et al.* (2019). The permafrost dynamics
203 from 1980 to 2009 for all scenarios were simulated by the modified Noah LSM following a
204 30-year spin-up using the repeating forcing data of 1979 as forcing. The temporal and spatial
205 resolutions of the simulations are 3 hr and 0.1° × 0.1°. The modeling depth amounts to 15.2
206 m with 18 soil layers. The time series of key thermal indicators for permafrost, including
207 permafrost area, active layer thickness (ALT) and mean annual ground temperature (MAGT),
208 were computed for each modeling cell. As per its definition, the MAGT was calculated as
209 the interpolated ground temperature of the first depth in a permafrost cell at which the annual
210 temperature amplitude is less than 0.2 °C. A cell was designated as permafrost provided that
211 the maximum temperature of any soil layer in the cell was ≤0 °C for two consecutive years.
212 The Albers equal-area conic projection was applied to ensure no area distortion during the
213 computation.

214 The summer scenarios were compared against the baseline to assess the impacts of
215 summer temperature changes on permafrost indicators, whereas the winter scenarios to
216 assess the effects of winter temperature changes. The relative importance of seasonal climate
217 warming was then identified through inter-comparisons between seasonal scenario groups in
218 term of consistency and digression. As shown in Table 1, there are only two stages in each

hypothetical scenario that differ from the baseline stages, i.e., C2 and C3 in SR1 and SR4; C1 and C3 in SR2 and SR5; and C1 and C2 in SR3 and SR6. Thus, we focused on the differences of these two stages (varied stages). By subtracting the baseline results from each hypothetical scenario results, we calculated the differences for these varied stages and drew the corresponding boxplots for the selected indicators. For example, if greater differences in a given indicator are showed in the boxplots for winter scenarios, it indicates that the indicator is more sensitive to winter temperature changes. Spatially, we drew difference maps relative to the baseline for the ending year of the two varied stages. If greater differences are detected in, for example, winter scenarios, it indicates that winter temperature changes exert a greater impact on the indicator than the summer temperature changes do.

We then quantified the contributions of unit degree of seasonal climate warming to the changes in ALT and MAGT. The area indicator was not included because the disappearance of permafrost mainly occurred in small transition areas between permafrost and seasonally frozen ground, not so sensitive as the others in response to climate warming. Based on the temporal series of the ALT and MAGT in all scenarios, we obtained their stage averages. Then, for each hypothetical scenario and the baseline, we calculated the differences with respect to indicator's stage average. Similarly, we computed the differences between hypothetical scenarios and the baseline with respect to averaged air temperature in the given season. The contribution of unit degree seasonal warming to the changes in the specific permafrost indicator is defined as the ratio of the difference in the indicator average over the difference in the air temperature average for the season considered. Since there are two

varied stages in each scenario pair, two contribution quantities could be calculated for the first and second varied stages. For the scenarios with two successive varied stages such as, SR1, SR4 and SR6, the second quantity was modified as a mean of contributions of both stages in recognition of the influences of the first stage extending into the second. The mean contribution is the quotient of the averaged indicator difference by the averaged seasonal temperature in the two successive varied stages.

3. Results and Discussion

3.1. Spatial-temporal differences in seasonal climate warming

The mean annual air temperature on the QTP exhibited an obvious increasing trend in the 1980-2000s (black line in Figure 1a). The average rate of increase was 0.46 °C/decade and was consistent with the one based on field observations (*Duan and Xiao,* 2015). Strong seasonal variations in warming rate were found. The annual change rate of winter temperature (blue line in Figure 1a) was 0.66 °C/decade, over twice the rate of summer temperature (red line in Figure 1a). On a decadal scale, seasonal differences in change rate were also apparent (Figure 1b). Winter warming tended to speed up through the three decades, exceeding summer warming in the last decade in terms of change rate. In the 2000s, the warming rate across winters were about three times more than the rate in summers. Despite a slowed summer warming rate than that in the previous stage (1990s), summer temperatures still kept rising in the 2000s. In the 1990s, there was the highest warming rate in summers along with the largest interquartile range. This decade was characterized by

highly fluctuating annual summer air temperatures (red line in Figure 1a) and the presence of extreme temperatures in this decade led to the highest linear rate.

Figure 1. Air temperature variabilities during the 1980s–2000s on the Qinghai-Tibet Plateau (QTP). (a) Temporal changes of winter (November–April), summer (May–October), and mean annual air temperature computed from the China Meteorological Forcing Dataset. CR and R denote an annual change rate (°C/decade) and correlation coefficient, respectively. (b) Boxplot showing changes in winter and summer air temperatures in three decades: 1980s, 1990s and 2000s. The boxes represent 25–75% quartiles and the whiskers are 1.5 interquartile ranges from the medians shown as the black lines in boxes. The black dots indicate mean values, and the star symbol (*), an outlier value. The values labeled over the boxes are decadal change rates (°C/decade). (c) and (d) Spatial patterns of change rates in (c) winters and (d) summers of 1980s–2000s across the QTP. The change rate is determined by the slope of a linear trend.

Figures 1c and 1d present the spatial distributions of change rates in winter and summer, respectively. It is clear that the most regions on the QTP have experienced pronounced warming in both seasons, except the northwest QTP and some small areas on the southeast presenting opposite patterns. The most notable warming in both seasons were found in the southwest QTP. Meanwhile, the spatial patterns differed by season. Overall, the winter warming rate over the entire plateau was considerably higher than the summer warming rate, in particular on the central and southern QTP. The cooling trend on the northwest QTP in contrast to the general trend on the QTP was especially pronounced in summer (Figure 1d).

It is likely strongly connected with weakened Indian monsoon and strengthened westerlies, which penetrate into the inner regions of the plateau and bring cold-wet water vapor (*Chen et al.,* 2008; *Li et al.,* 2019). These results confirm the distinction of winter warming over summer warming in the context of climate warming over the QTP.

3.2. Permafrost responses to seasonal climate warming

Figure 2 illustrates the temporal changes in permafrost indicators (permafrost area, ALT and MAGT) simulated under the six hypothetical scenarios and the baseline scenario. The results show marked differences in the permafrost responses to various seasonal climate warming conditions. The differences relative to the baseline were positive in the SR2, SR3 and SR6 scenarios, indicating more severe permafrost degradation under those scenarios than under the baseline scenario (Figures 2d ~ 2f). It is logical as most of those scenarios have higher temperature segments than the baseline as shown in Table 1. Although there are a warmer C1 and a colder C2 in SR3 compared to the baseline, the overall temperature of C1 and C2 is still higher than the baseline. The negative differences in SR1, SR4 and SR5 indicate more developed permafrost than in the baseline, attributable to their lower temperature segments in the scenario settings. It is obvious permafrost changes in the winter scenarios (SR4–SR6) departed more from the baseline results than in the summer scenarios (SR1–SR3). The maximal deviations appeared in SR4 and SR6, both winter scenarios. The occurrence of larger departures from the baseline curves in winter scenarios is suggestive of more thermal sensitivity of permafrost to changes in winter temperature. Note that even though warming persisted through the entire period, a short-term reversal after 2000 coincided in all seven

scenarios, which were captured by all indicators. The ALTs rapidly declined in 2000–2004 and the extent of permafrost has expanded in 2001–2005. The MAGTs started to decline from 2005, several years after the decline in ALT. Obvious hysteresis among those indicators was detected. Such reversal is believed to be associated with increasing precipitation occurred in 1998–2005 (*Zhang et al.*, 2021). This implies that precipitation changes are also important in modulating permafrost thermal regimes. Zhang *et al*. (2021) reported that increased summer precipitation reduces permafrost thermal responses to climate warming, especially in arid and semi-arid areas on the QTP.

Figure 2. Temporal changes of permafrost indicators during the 1980s–2000s under six hypothetical scenarios and the baseline. (a) Permafrost area. (b) Active layer thickness (ALT) in permafrost regions. (c) Mean annual ground temperature (MAGT) in permafrost regions. The baseline represents the permafrost changes under historical climatic conditions. The summer scenarios (SR1–SR3) hold constant decadal summer temperatures that represent low, high and medium levels of summer warming, respectively. The winter scenarios (SR4–SR6) hold constant decadal winter temperatures representing low, medium and high levels of winter warming, respectively. (d) ~ (f) Differences between the results of hypothetical scenarios and the baseline in permafrost area, ALT, and MAGT during the two varied stages, respectively, expressed in the boxplots. The differences reflect the impacts of summer/winter temperature changes relative to the baseline. The boxes represent 25–75% quartiles and the whiskers are 1.5 interquartile ranges from the medians shown in black lines in the boxes. The black dots indicate mean values, and the star symbol (*), an outlier value.

Spatial distributions of the differences in permafrost indicators under hypothetical scenarios with respect to the baseline results revealed generally the same directions in most regions (Figures 3 ~ 5) as did the temporal analysis. Unlike the general warming in most areas of QTP, the northwest QTP (marked with No.1 in Figures 3 ~ 5) presented a contradictory pattern due to the regional cooling in summer. In both the summer and winter scenarios, prevalent negative differences against the baseline appeared in SR1 and SR4, while largest positive differences appeared in SR3 and SR6. The differences in SR2 and SR5 are in-between. Both SR1 and SR4 represent lower temperature conditions than the baseline in the summer and winter scenarios, respectively, with a same rank of low in their own groups. Lower MAGTs and thinner ALTs as well as increased permafrost area (top rows in Figures 3 ~ 5) were simulated as expected in SR1 and SR4 relative to the baseline, with more negative areas occurring in SR4. By comparing the SR1 and SR4 results, it could lead to the implications that low winter temperature (SR4) is more conducive to permafrost growth than low summer temperature (SR1). In contrast, SR3 and SR6 represent higher temperature conditions in summers (medium level) and winters (high level) with respect to the baseline, respectively. Considerable permafrost degradation has been occurred in both scenarios, as indicated by higher MAGT, thickened ALT and area shrinkage prevalent on the plateau except the northwest QTP (bottom rows in Figures 3 ~ 5). The most severe degradation was observed in SR6, as evidenced by dramatically increased MAGT in SR6 (Figure 3f). Since the rates of winter warming in SR3 and SR6 differ, we cannot easily conclude that the contribution of per degree warming in winter to the thermal regimes of permafrost is larger than that in summer. However, the fact is the fixed seasonal temperatures

345 in both scenarios are from the same C3 phase, where winter warming is more pronounced
346 than summer warming. Given disparate seasonal warming rates, the impacts of winter
347 warming on permafrost were simulated to be larger than summer warming as demonstrated
348 between SR3 and SR6.

349 Similar findings can also be obtained by examining the scenario results on different stages.
350 The scenarios SR1, SR2, SR3, and SR6 have same winter segments in C3 identical to the
351 counterpart in the baseline, and they generally differ in the C1 and C2 stages from the
352 baseline and from each other. Consequently, the simulated indicators for those scenarios
353 varied considerably in C1 and C2, whereas they tended to converge to the baseline curve in
354 C3 (Figures 2a ~ 2c), even though the summer segments in C3 were not identical. This
355 convergence was even pronounced in terms of MAGT. In C3, the four scenario curves had
356 high correlation with the baseline curve with coefficients of 0.77, 0.73, 0.99 and 0.82,
357 respectively. At the ending year of C3, the MAGT values in the four scenarios were very
358 close with an exception in SR2. In contrast, the scenarios SR3, SR4, SR5, and SR6 have
359 same summer segments in C3, also identical to the counterpart in the baseline. The indicator
360 curves of those scenarios, however, deviated from each other in C3. The greatest departures
361 from the baseline curves occurred in SR4 and SR5. The two scenarios own lower winter
362 temperature segments (C1W and C2W) in C3 than C3W for other scenarios. The lower C3
363 winter temperatures had the MAGT curves dropped far below the baseline, signifying their
364 roles in affecting permafrost thermal regime. The different behaviors of those two groups in
365 the C3 stage consistently imply the thermal state of permafrost on the QTP is particularly
366 sensitive to winter warming.

Figure 3. Difference maps of the MAGT on the QTP permafrost regions between hypothetical scenarios and the baseline. (a) ~ (c) for summer scenarios (SR1 to SR3); (d) ~ (f) for winter scenarios (SR4 to SR6). The dark blue indicates largest negative differences and the red, positive differences. The No.1 rectangle indicates an atypical region inconsistent with the most regions on the QTP. The No.2 and No.3 regions are the Three River Source region and the Qiangtang High Plateau, respectively.

3.3. Regional thermal degradation induced by seasonal climate warming

Remarkable differences in space was found under winter scenarios (SR4–SR6) in the Three River Source region (No. 2 in Figures 3 ~ 5) and on the Qiangtang High Plateau (No.3 in Figures 3 ~ 5). The latter is located within the alpine continuous permafrost region of QTP. The differences were especially clear in the MAGT difference maps (Figure 3). It indicates that permafrost in both regions is particularly sensitive to winter temperature change and vulnerable to winter warming. Among the winter scenarios, negative differences in both regions were observed in both SR4 and SR5, whereas positive differences appeared only in SR6. Since the SR4–SR6 scenarios reflect winter temperature changes in 1980s, 1990s, 2000s, respectively, it can be reasonably inferred that permafrost in those regions has experienced obvious thermal degradation induced by winter warming in the 2000s. The presented spatial patterns of MAGT difference in both regions are in broad consistency with the spatial patterns of winter temperature changes (Figure 1c).

The regional warming in permafrost on the Qiangtang High Plateau in the 2000s has been reported earlier (*Zhang et al.*, 2019). However, it failed in capturing the permafrost warming

388 occurred in the Three River Source region (marked as No.2). The reason for this could be
389 related to its oversimplified scenario setup. In reality, winter warming is not always
390 monotonously warming over winters, and more importantly, temperatures in summers also
391 varied year by year alongside winter warming. By taking a more sophisticated scenario
392 design like the one developed in this study, we found severe thermal degradation in the
393 Three River Source region in the 2000s as indicated by the MAGT differences, and even
394 some portions of permafrost in this region had degraded into seasonally frozen ground (No.2
395 in Figure 5f). It would consequently affect water availability in this region and peripheries
396 and lead to tremendous impacts as the Three River Source region is the source area for the
397 important Asian rivers: the Yangtze, Yellow, and Mekong rivers. One of possible
398 consequences of increasing streamflow in the nearby regions have been demonstrated in a
399 recent study (*Chen et al.*, 2015). They connected the increased streamflow to greater
400 meltwater contributions from glaciers and permafrost without adequate evidence. Our
401 findings can provide important information which can be used to partially explain their
402 observations in this region.

403 Figure 4. Difference maps of the ALT on the QTP permafrost regions between hypothetical
404 scenarios and the baseline. The same notes as in Figure 3 are applied.

405 **3.4. Implications for permafrost responses to seasonal climate warming**

406 Note that the average summer warming rate in SR2 (high level) was higher than in SR3
407 (medium level). Surprisingly, more permafrost degradation has been observed in SR3 than
408 SR2 (Figure 2). The fact behind this is that summer temperatures in SR3 (representing

summers of 2000s, red box in Figure 1b) are with slightly higher mean and smaller quartiles, in contrast to high fluctuations in SR2 (representing summers of 1990s, magenta box in Figure 1b). This finding seems to suggest that steady warming as in SR3 is more likely to induce permafrost degradation than highly fluctuating warming even at a higher warming rate as in SR2. The below-the-average temperatures during a warming yet highly fluctuating period may inhibit thermal degradation in permafrost induced by the overall trend of warming. Meanwhile, the slightly higher mean of summer temperature in SR3 indicate, overall, more heat fluxes entering into the subsurface soils. Both lead to more permafrost degradation occurred in SR3 than SR2 as presented in Figure 2.

It is generally agreed that the ALT is controlled by summer temperatures as it is measured in summer. In Figure 2b, if we ignore the changes after 1998 when precipitation predominately controlled, it can be seen that the ALT fluctuated with the change in summer temperature, reiterating the primary role of summer temperature changes in influencing the ALT. More specially, by looking at the differences in space, it is evident that the summer scenarios (SR1–SR3) caused larger and most extreme differences (Figure 4). However, moderate differences still could be observed in the maps of winter scenarios, even if the winter scenarios had the same summer temperatures as the baseline. In Figure 2e, the mean differences in ALT for SR4 and SR6 (both winter scenarios) were close to those for the corresponding summer scenarios. But from the temporal series of ALT (Figure 2b), the largest increase in ALT before 1999 against the baseline occurred in SR6. Recalling that SR6 is the scenario that all winter temperatures change at the highest warming rate, i.e., the one

of the 2000s, it can be reasonably inferred that rapid winter warming may also exert significant influence on the ALT, as demonstrated by the SR6 curve in Figure 2b surpassing any summer scenarios in the late C2 stage. It can be well explained, in theory, winter temperature changes alter the onset time of soil freezing process and the storage of soil "cold energy", and such effects extend to the following thawing period, thus affecting the energy budget of frozen soils on an annual basis (*Zhang et al.*, 2019). Consequently, winter warming affects the ALT in a delayed manner.

Figure 5. Spatial distributions and transition of frozen ground type from the type simulated in the baseline to the type in hypothetical scenarios. (a) ~ (c) for summer scenarios (SR1 to SR3); (d) ~ (f) for winter scenarios (SR4 to SR6). The No.1 rectangle marks a pronounced atypical region affected by regional climatic conditions that deviate from the general conditions over the entire plateau. The No.2 rectangle indicates the Three River Source region.

Unlike the obvious changes in MAGT, changes in permafrost area under different scenarios were rather small as shown in Figure 2a and 2d. The transition maps of the frozen ground types simulated (Figure 5) indicate that most permafrost on the northern QTP remained stable in type during the study period. A small number of transitions were mostly occurred around the boundaries of the continuous and island permafrost regions in the southwest QTP. These results are in line with the findings that it usually takes decades or even longer to completely melt thermally stable permafrost and only warm permafrost is at high risk of thawing (*Sun et al.*, 2020). Both summer and winter scenarios (SR3 and SR6)

showed same pattern. This implies warm permafrost in those regions is much more sensitive to climate changes in all seasons and is becoming more at risk under a persistently warming climate.

3.5. Contributions per unit of seasonal climate warming to changes in permafrost

The contributions from summer and winter climate warming to the changes in permafrost indicators (ALT and MAGT) are quantified separately, as listed in Table 2. The results show if average summer air temperature in permafrost regions increases by 1 ℃, the average ALT increases by 0.35 m, with a range of 0.08 to 0.71 m. For one-degree winter warming, the average ALT increases 0.16 m and ranges from 0.03 to 0.30 m. Similarly, one degree in average summer temperature rising leads to 0.20℃ increase in MAGT, with a range of 0.06 to 0.45 ℃, and in winter, it leads to a mean of 0.13 ℃ increase in MAGT, ranging from 0.02 to 0.22 ℃. SR3 has two successive stages with upward and downward temperature changes compared to the baseline, and the second stage will be highly influenced by the preceding one. Thus, the second stage of SR3 was excluded in calculating average contributions. The unit contribution of summer climate warming to permafrost changes with respect to ALT and MAGT was estimated to be larger than that of winter warming. However, it should be noted that despite of a smaller unit contribution of winter warming, winter warming had much larger magnitude (1.46 ℃) than summer warming (0.52 ℃) in the 2000s (Figure 1b). As a result, winter warming in the 2000s exerts more prominent impact on permafrost changes than summer warming.

Table 2. Contributions of unit degree warming of average winter and summer air

472 temperatures in permafrost regions over the QTP to the changes in ALT and MAGT.

473 **4. Conclusions**

474 We quantified the isolated contributions of seasonal climate warming to permafrost
475 thermal responses over the QTP through a set of contrasting numerical scenarios and the
476 modified Noah LSM. Simulation results show that the permafrost thermal regime was highly
477 sensitive to winter air temperature change. Permafrost in the Three River Source region and
478 on the Qiangtang High Plateau has undergone significant regional thermal degradation
479 induced by rapid winter climate warming in the 2000s. The contribution of unit degree
480 warming in summer to permafrost changes with respect to ALT and MAGT was estimated to
481 be larger than that in winter. One degree rising in average summer air temperature in
482 permafrost regions of QTP leads to 0.35 m increase in ALT and 0.20 ℃ increase in MAGT,
483 whereas average winter climate warming by 1 ℃ leads to 0.16 m increase in ALT and 0.13 ℃
484 increase in MAGT. But it should be noticed that despite of a smaller unit contribution of
485 winter climate warming to permafrost changes, the overall impact of winter climate warming
486 has exceeded summer warming in the 2000s due to a triple larger rate of winter climate
487 warming than summer warming in this decade. We have also revealed permafrost is mostly
488 likely susceptible to a steady warming climate than a warming yet highly fluctuating climate.
489 Summer air temperature changes mainly influence the ALT, but our findings also show
490 winter temperature changes may considerably affect the ALT on an annual basis. While
491 permafrost in most QTP regions remained stable in type under a warming climate, the island
492 permafrost on the southwestern QTP was at high risk of degradation into seasonally frozen

493 ground given warming in any seasons.

494 In addition to seasonal climate warming, precipitation is also a key factor that cannot be
495 ignored in regulating the thermal regimes of permafrost as manifested in the scenario
496 simulations. When predicting future permafrost changes on the QTP, the effects of seasonal
497 warming and increased precipitation should be simultaneously considered, in particular
498 when precipitation is projected to continually increase in the future (*Su et al.*, 2013).

499 **Acknowledgments**

500 This work was supported by the grants of the National Natural Science Foundation of China
501 (41931180 and 41971074) and the National Key R&D Program of China
502 (2017YFA0603603). It also received the support from the Postgraduate Research & Practice
503 Innovation Program of Jiangsu Province (KYCX21_1345). We thank the Tibetan Plateau
504 Data Center (http://data.tpdc.ac.cn) and the National Cryosphere Desert Data Center
505 (http://www.ncdc.ac.cn) for providing data. The authors would like to thank the anonymous
506 reviewers for the constructive feedback and some special thanks go to the reviewer who
507 thoroughly edited the language for this manuscript.

508 **Data Availability Statement**

509 The results and associated data in this study can be obtained from the OSF repository
510 (https://doi.org/10.17605/osf.io/jvy3e).

511 **References**

512 Chadburn, S. E., Burke, E. J., Cox, P. M., Friedlingstein, P., Hugelius, G., Westermann, S.
513 (2017), An observation-based constraint on permafrost loss as a function of global

warming, *Nature Climate Change*, *7*(5), 340-344, https://doi.org/10.1038/nclimate3262.

Chen, D., Xu, B., Yao, T., Guo, Z., Cui, P., Chen, F. et al. (2015), Assessment of past, present and future environmental changes on the Tibetan Plateau (in Chinese), *Chinese Science Bulletin*, *60*(32), 3025-3035, https://doi.org/10.1360/N972014-01370.

Chen, F., Yu, Z., Yang, M., Ito, E., Wang, S., Madsen, D. B. et al. (2008), Holocene moisture evolution in arid central Asia and its out-of-phase relationship with Asian monsoon history, *Quaternary Science Reviews*, *27*(3-4), 351-364, https://doi.org/10.1016/j.quascirev.2007.10.017.

Chen, W., Jiang, Z., Li, L. (2011), Probabilistic Projections of Climate Change over China under the SRES A1B Scenario Using 28 AOGCMs, *Journal of Climate*, *24*(17), 4741-4756, https://doi.org/10.1175/2011JCLI4102.1.

Chen, Y., Yang, K., He, J., Qin, J., Shi, J., Du, J. et al. (2011), Improving land surface temperature modeling for dry land of China, *Journal of Geophysical Research*, *116*(D20), D20104, https://doi.org/10.1029/2011JD015921.

Cheng, G., Wu, T. (2007), Responses of permafrost to climate change and their environmental significance, Qinghai-Tibet Plateau, *Journal of Geophysical Research*, *112*(F2), F2S-F3S, https://doi.org/10.1029/2006JF000631.

Cheng, G., Zhao, L., Li, R., Wu, X., Sheng, Y., Hu, G. et al. (2019), Characteristic, changes and impacts of permafrost on Qinghai-Tibet Plateau (in Chinese), *Chinese Science Bulletin*, *64*(27), 2783-2795, https://doi.org/10.1360/TB-2019-0191.

536 Chiang, J. C. H., Fung, I. Y., Wu, C., Cai, Y., Edman, J. P., Liu, Y. et al. (2015), Role of
537 seasonal transitions and westerly jets in East Asian paleoclimate, *Quaternary Science*
538 *Reviews*, *108*, 111-129, https://doi.org/10.1016/j.quascirev.2014.11.009.
539 Duan, A., Xiao, Z. (2015), Does the climate warming hiatus exist over the Tibetan Plateau?
540 *Scientific Reports*, *5*(1), 13711, https://doi.org/10.1038/srep13711.
541 Duan, A. M., Wu, G. X. (2005), Role of the Tibetan Plateau thermal forcing in the summer
542 climate patterns over subtropical Asia, *Climate Dynamics*, *24*(7-8), 793-807,
543 https://doi.org/10.1007/s00382-004-0488-8.
544 Duan, J., Li, L., Fang, Y. (2015), Seasonal spatial heterogeneity of warming rates on the
545 Tibetan Plateau over the past 30 years, *Scientific Reports*, *5*(1), 11725,
546 https://doi.org/10.1038/srep11725.
547 Guo, D., Wang, H., Li, D. (2012), A projection of permafrost degradation on the Tibetan
548 Plateau during the 21st century, *Journal of Geophysical Research: Atmospheres*,
549 *117*(D5), D5106, https://doi.org/10.1029/2011JD016545.
550 Immerzeel, W. W., van Beek, L. P. H., Bierkens, M. F. P. (2010), Climate change will affect
551 the Asian water towers, *Science*, *328*(5984), 1382-1385,
552 https://doi.org/10.1126/science.1183188.
553 Jin, H., Li, S., Li, X., Cheng, G., Shaoling, W. (2000), Permafrost and climatic change in
554 China, *Global and Planetary Change*, *26*(4), 387-404,
555 https://doi.org/10.1016/S0921-8181(00)00051-5.

Kang, S., Xu, Y., You, Q., Flügel, W., Pepin, N., Yao, T. (2010), Review of climate and cryospheric change in the Tibetan Plateau, *Environmental Research Letters*, *5*(1), 15101, https://doi.org/10.1088/1748-9326/5/1/015101.

Kuang, X., Jiao, J. J. (2016), Review on climate change on the Tibetan Plateau during the last half century, *Journal of Geophysical Research: Atmospheres*, *121*(8), 3979-4007, https://doi.org/10.1002/2015JD024728.

Li, X., Cheng, G., Jin, H., Kang, E., Che, T., Jin, R. et al. (2008), Cryospheric change in China, *Global and Planetary Change*, *62*(3-4), 210-218, https://doi.org/10.1016/j.gloplacha.2008.02.001.

Li, X., Hou, J., Wang, M., He, Y. (2019), Influence of monsoon and westerlies on Holocene climate change in the Tibetan Plateau: Isotopic evidence (in Chinese), *Quaternary Sciences*, *39*(3), 678-686, https://doi.org/10.11928/j.issn.1001-7410.2019.03.14.

Liu, X., Zhang, M. (1998), Contemporary climatic change over the Qinghai-Xizang Plateau and its response to the green-house effect, *Chinese Geographical Science*, *8*(4), 289-298, https://doi.org/10.1007/s11769-997-0034-9.

Liu, X., Chen, B. (2000), Climatic warming in the Tibetan Plateau during recent decades, *International Journal of Climatology*, *20*(14), 1729-1742, https://doi.org/10.1002/1097-0088(20001130)20:14<1729::AID-JOC556>3.0.CO;2-Y.

Liu, X., Cheng, Z., Yan, L., Yin, Z. (2009), Elevation dependency of recent and future minimum surface air temperature trends in the Tibetan Plateau and its surroundings,

577 *Global and Planetary Change*, *68*(3), 164-174,
578 https://doi.org/10.1016/j.gloplacha.2009.03.017.
579 Ma, J., Zhang, T., Guan, X., Hu, X., Duan, A., Liu, J. (2019), The dominant role of snow/ice
580 albedo feedback strengthened by black carbon in the enhanced warming over the
581 Himalayas, *Journal of Climate*, *32*(18), 5883-5899,
582 https://doi.org/10.1175/JCLI-D-18-0720.1.
583 Molnar, P., Boos, W. R., Battisti, D. S. (2010), Orographic controls on climate and
584 paleoclimate of Asia: Thermal and mechanical roles for the Tibetan Plateau, *Annual*
585 *Review of Earth and Planetary Sciences*, *38*(1), 77-102,
586 https://doi.org/10.1146/annurev-earth-040809-152456.
587 Pan, B., Li, J. (1996), Qinghai-tibetan plateau: A driver and amplifier of the global climatic
588 change (in Chinese), *Journal of Lanzhou University (Natural Sciences)*, *32*(1),
589 108-115, https://doi.org/10. 13885/j.issn. 0455-2059.1996.01.024.
590 Pepin, N., Bradley, R. S., Diaz, H. F., Baraer, M., Caceres, E. B., Forsythe, N. et al. (2015),
591 Elevation-dependent warming in mountain regions of the world, *Nature Climate*
592 *Change*, *5*(5), 424-430, https://doi.org/10.1038/nclimate2563.
593 Rangwala, I., Sinsky, E., Miller, J. R. (2013), Amplified warming projections for high
594 altitude regions of the northern hemisphere mid-latitudes from CMIP5 models,
595 *Environmental Research Letters*, *8*(2), 24040,
596 https://doi.org/10.1088/1748-9326/8/2/024040.
597 Smith, L. C., Sheng, Y., MacDonald, G. M., Hinzman, L. D. (2005), Disappearing Arctic
598 lakes, *Science*, *308*(5727), 1429, https://doi.org/10.1126/science.1108142.

599 Su, F., Duan, X., Chen, D., Hao, Z., Cuo, L. (2013), Evaluation of the Global Climate
600 Models in the CMIP5 over the Tibetan Plateau, *Journal of Climate*, *26*(10),
601 3187-3208, https://doi.org/10.1175/JCLI-D-12-00321.1.
602 Sun, Z., Zhao, L., Hu, G., Qiao, Y., Du, E., Zou, D. et al. (2020), Modeling permafrost
603 changes on the Qinghai–Tibetan plateau from 1966 to 2100: A case study from two
604 boreholes along the Qinghai–Tibet engineering corridor, *Permafrost and Periglacial*
605 *Processes*, *31*(1), 156-171, https://doi.org/10.1002/ppp.2022.
606 Wang, S., Jin, H., Li, S., Zhao, L. (2000), Permafrost degradation on the Qinghai-Tibet
607 Plateau and its environmental impacts, *Permafrost and Periglacial Processes*, *11*(1),
608 43-53,
609 https://doi.org/10.1002/(SICI)1099-1530(200001/03)11:1<43::AID-PPP332>3.0.CO;
610 2-H.
611 Wu, T., Zhao, L., Li, R., Wang, Q., Xie, C., Pang, Q. (2013), Recent ground surface
612 warming and its effects on permafrost on the central Qinghai-Tibet Plateau,
613 *International Journal of Climatology*, *33*(4), 920-930,
614 https://doi.org/10.1002/joc.3479.
615 Wu, X., Nan, Z., Zhao, S., Zhao, L., Cheng, G. (2018), Spatial modeling of permafrost
616 distribution and properties on the Qinghai-Tibet Plateau, *Permafrost and Periglacial*
617 *Processes*, *29*(2), 86-99, https://doi.org/10.1002/ppp.1971.
618 Xu, X., Lu, C., Shi, X., Gao, S. (2008), World water tower: An atmospheric perspective,
619 *Geophysical Research Letters*, *35*(20), https://doi.org/10.1029/2008GL035867.

Yanai, M., Li, C., Song, Z. (1992), Seasonal heating of the Tibetan Plateau and its effects on the evolution of the Asian summer monsoon, *Journal of the Meteorological Society of Japan. Ser. II*, *70*(1B), 319-351, https://doi.org/10.2151/jmsj1965.70.1B_319.

Yao, T., Thompson, L., Yang, W., Yu, W., Gao, Y., Guo, X. et al. (2012), Different glacier status with atmospheric circulations in Tibetan Plateau and surroundings, *Nature Climate Change*, *2*(9), 663-667, https://doi.org/10.1038/nclimate1580.

Yao, T., Xue, Y., Chen, D., Chen, F., Thompson, L., Cui, P. et al. (2019), Recent Third Pole's rapid warming accompanies cryospheric melt and water cycle intensification and interactions between monsoon and environment: Multidisciplinary approach with observations, modeling, and analysis, *Bulletin of the American Meteorological Society*, *100*(3), 423-444, https://doi.org/10.1175/BAMS-D-17-0057.1.

You, Q., Kang, S., Pepin, N., Flügel, W., Sanchez-Lorenzo, A., Yan, Y. et al. (2010), Climate warming and associated changes in atmospheric circulation in the eastern and central Tibetan Plateau from a homogenized dataset, *Global and Planetary Change*, *72*(1-2), 11-24, https://doi.org/10.1016/j.gloplacha.2010.04.003.

You, Q., Ren, G., Fraedrich, K., Kang, S., Ren, Y., Wang, P. (2013), Winter temperature extremes in China and their possible causes, *International Journal of Climatology*, *33*(6), 1444-1455, https://doi.org/10.1002/joc.3525.

Zhang, G., Nan, Z., Wu, X., Ji, H., Zhao, S. (2019), The role of winter warming in permafrost change over the Qinghai-Tibet Plateau, *Geophysical Research Letters*, *46*(20), 11261-11269, https://doi.org/10.1029/2019GL084292.

641 Zhang, G., Nan, Z., Zhao, L., Liang, Y., Cheng, G. (2021), Qinghai-Tibet Plateau wetting
642 reduces permafrost thermal responses to climate warming, *Earth and Planetary*
643 *Science Letters*, *562*, 116858, https://doi.org/10.1016/j.epsl.2021.116858.
644 Zhang, R., Su, F., Jiang, Z., Gao, X., Guo, D., Ni, J. et al. (2015), An overview of projected
645 climate and environmental changes across the Tibetan Plateau in the 21st century (in
646 Chinese), *Chinese Science Bulletin*, *60*(32), 3036-3047,
647 https://doi.org/10.1360/N972014-01296.
648 Zhong, L., Su, Z., Ma, Y., Salama, M. S., Sobrino, J. A. (2011), Accelerated changes of
649 environmental conditions on the Tibetan Plateau caused by climate change, *Journal*
650 *of Climate*, *24*(24), 6540-6550, https://doi.org/10.1175/JCLI-D-10-05000.1.

Table captions

Table 1. Baseline and hypothetical scenarios by assembling decadal seasonal segments coming from the three decadal stages in the historic records.

Group	Scenario	Scenario segments			Temperature level	Differences from the
		C1 (1980s)	C2 (1990s)	C3 (2000s)	of the fixed season	Baseline (SR-Baseline)
Historical	Baseline	C1S_C1W	C2S_C2W	C3S_C3W		
Summer scenarios	SR1	C1S_C1W	↓C1S_C2W	↓C1S_C3W	Low	C1S-C2S & C3S
	SR2	↑C2S_C1W	C2S_C2W	↑C2S_C3W	High	C2S-C1S, C2S-C3S
	SR3	↑C3S_C1W	↓C3S_C2W	C3S_C3W	Medium	C3S-C1S & C2S
Winter scenarios	SR4	C1S_C1W	C2S_C1W↓	C3S_C1W↓	Low	C1W-C2W & C3W
	SR5	C1S_C2W↑	C2S_C2W	C3S_C2W↓	Medium	C2W-C1W, C2W-C3W
	SR6	C1S_C3W↑	C2S_C3W↑	C3S_C3W	High	C3W-C1W & C2W

Notes: SR1–SR6 are hypothetical scenarios. The summer segments of C1S, C2S, C3S, and winter segments of C1W, C2W, C3W originate from the historical records. The arrow marks near the segments indicate those segments are distinct from the corresponding segments in the baseline. The symbol ↓ denotes lower decadal air temperature conditions compared to the counterpart in the baseline, while ↑ denotes higher temperature conditions. The relative temperature levels of the fixed seasons (e.g., C1S is holding constant in SR1) are ranked according to its decadal change rate within its group.

Table 2. Contributions of unit degree warming of average winter and summer air temperatures in permafrost regions over the QTP to the changes in ALT and MAGT.

Group	Scenario	Contribution to ALT (m/°C)	Contribution to MAGT (°C/°C)
Summer scenarios	SR1	0.25(0.44)	0.06(0.13)
	SR2	0.29(0.08)	0.14(0.22)
	SR3	0.71(–)	0.45(–)
Winter scenarios	SR4	0.17(0.24)	0.11(0.19)
	SR5	0.03(0.30)	0.02(0.22)
	SR6	0.09(0.12)	0.08(0.15)

Notes: The value parenthesized represents the contribution on the second different stage or the averages of contributions if otherwise the two different stages are successive. The second quantity for SR3 is meaningless and marked by the symbol (–).

Figure captions

Figure 1. Air temperature variabilities during the 1980s–2000s on the Qinghai-Tibet Plateau (QTP). (a) Temporal changes of winter (November–April), summer (May–October), and mean annual air temperature computed from the China Meteorological Forcing Dataset. CR and R denote an annual change rate (°C/decade) and correlation coefficient, respectively. (b) Boxplot showing changes in winter and summer air temperatures in three decades: 1980s, 1990s and 2000s. The boxes represent 25–75% quartiles and the whiskers are 1.5 interquartile ranges from the medians shown as the black lines in boxes. The black dots indicate mean values, and the star symbol (*), an outlier value. The values labeled over the boxes are decadal change rates (°C/decade). (c) and (d) Spatial patterns of change rates in (c) winters and (d) summers of 1980s–2000s across the QTP. The change rate is determined by the slope of a linear trend.

Figure 2. Temporal changes of permafrost indicators during the 1980s–2000s under six hypothetical scenarios and the baseline. (a) Permafrost area. (b) Active layer thickness (ALT) in permafrost regions. (c) Mean annual ground temperature (MAGT) in permafrost regions. The baseline represents the permafrost changes under historical climatic conditions. The summer scenarios (SR1–SR3) hold constant decadal summer temperatures that represent low, high and medium levels of summer warming, respectively. The winter scenarios (SR4–SR6) hold constant decadal winter temperatures representing low, medium and high levels of winter warming, respectively. (d) ~ (f) Differences between the results of hypothetical scenarios and the baseline in permafrost area, ALT, and MAGT during the two varied stages, respectively, expressed in the boxplots. The differences reflect the impacts of summer/winter

temperature changes relative to the baseline. The boxes represent 25–75% quartiles and the whiskers are 1.5 interquartile ranges from the medians shown in black lines in the boxes. The black dots indicate mean values, and the star symbol (*), an outlier value.

Figure 3. Difference maps of the MAGT on the QTP permafrost regions between hypothetical scenarios and the baseline. (a) ~ (c) for summer scenarios (SR1 to SR3); (d) ~ (f) for winter scenarios (SR4 to SR6). The dark blue indicates largest negative differences and the red, positive differences. The No.1 rectangle indicates an atypical region inconsistent with the most regions on the QTP. The No.2 and No.3 regions are the Three River Source region and the Qiangtang High Plateau, respectively.

Note: Please place Figure 3 in landscape orientation

Figure 4. Difference maps of the ALT on the QTP permafrost regions between hypothetical scenarios and the baseline. The same notes as in Figure 3 are applied.

Note: Please place Figure 4 in landscape orientation

Figure 5. Spatial distributions and transition of frozen ground type from the type simulated in the baseline to the type in hypothetical scenarios. (a) ~ (c) for summer scenarios (SR1 to SR3); (d) ~ (f) for winter scenarios (SR4 to SR6). The No.1 rectangle marks a pronounced atypical region affected by regional climatic conditions that deviate from the general conditions over the entire plateau. The No.2 rectangle indicates the Three River Source region.

Note: Please place Figure 5 in landscape orientation

Figure 1.

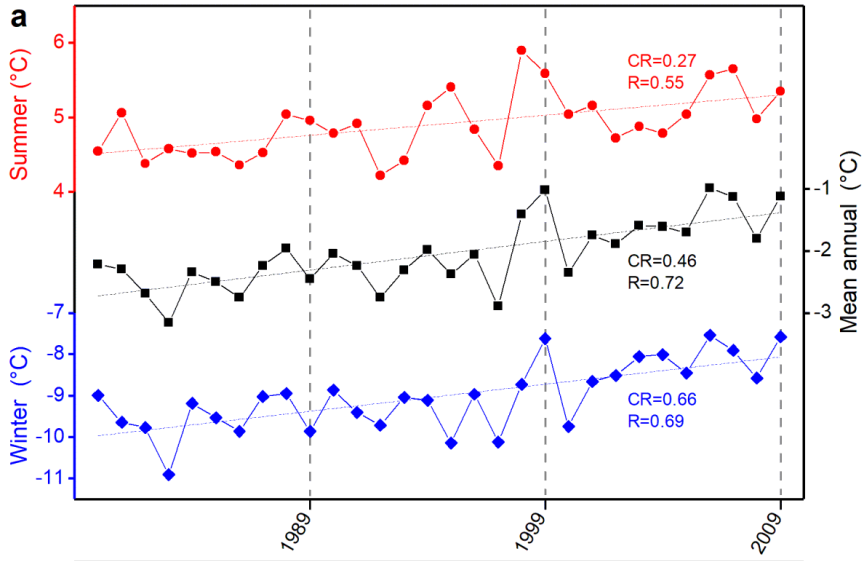
a
Summer (°C)
Winter (°C)
Mean annual (°C)
CR=0.27
R=0.55
CR=0.46
R=0.72
CR=0.66
R=0.69
1989
1999
2009

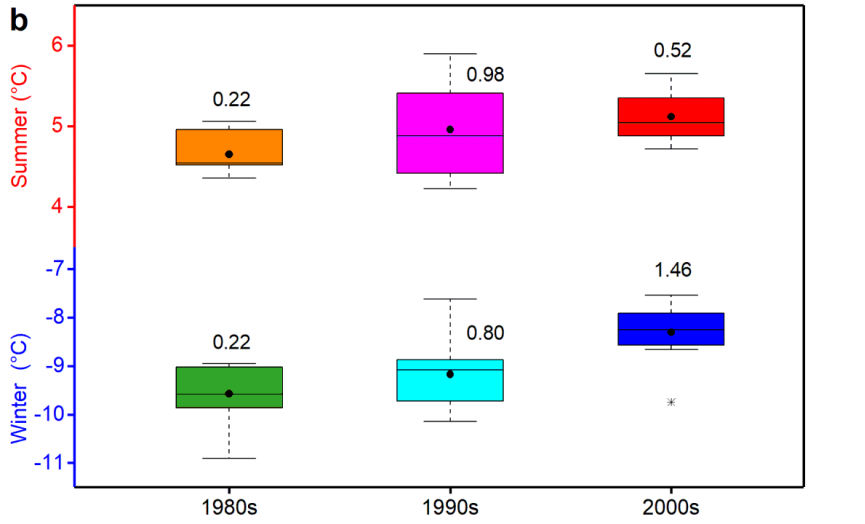
b
Summer (°C)
Winter (°C)
0.22
0.98
0.52
0.22
0.80
1.46
1980s
1990s
2000s

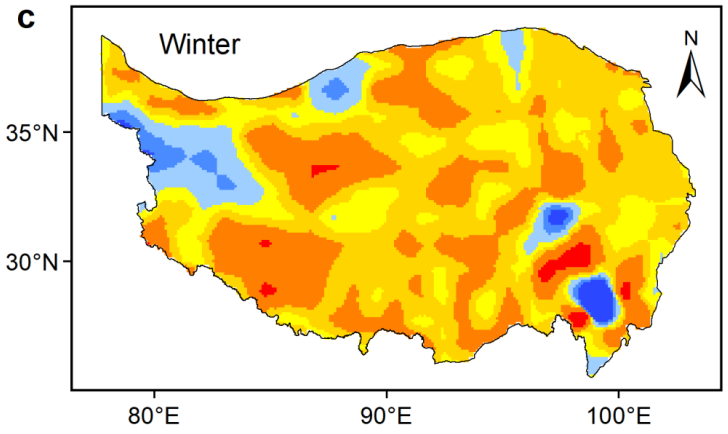
c
Winter
N
35°N
30°N
80°E
90°E
100°E

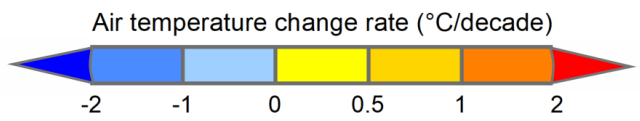
Air temperature change rate (°C/decade)
-2
-1
0
0.5
1
2

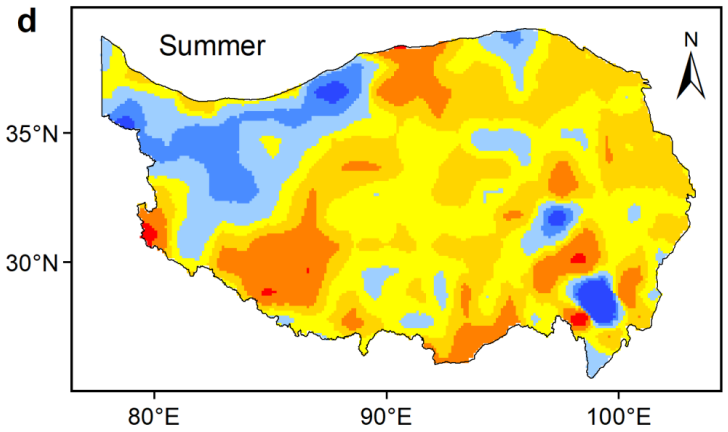
d
Summer
N
35°N
30°N
80°E
90°E
100°E

Figure 2.

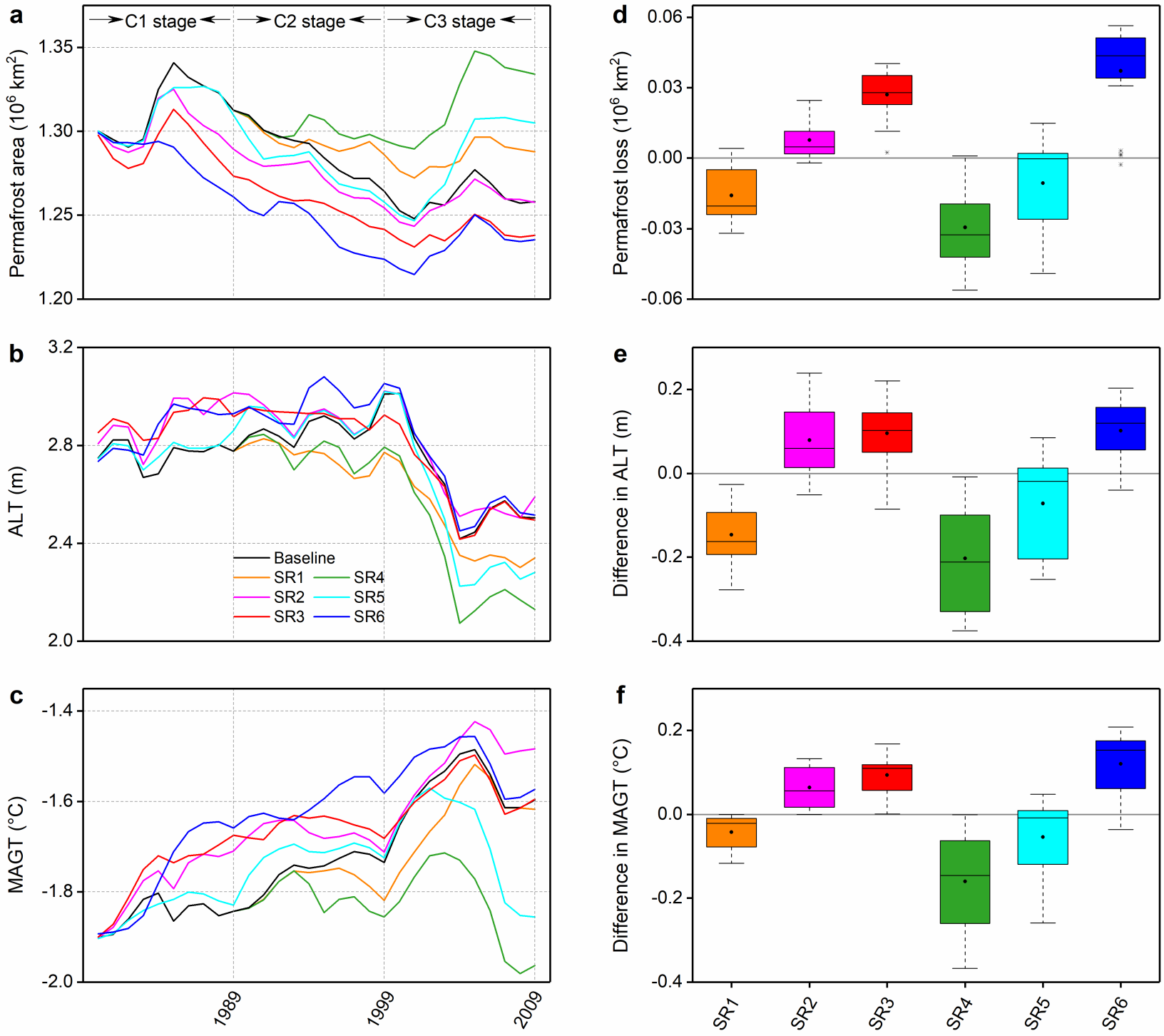
a
C1 stage
C2 stage
C3 stage
Permafrost area (10^6 km^2)
1.35
1.30
1.25
1.20
b
ALT (m)
3.2
2.8
2.4
2.0
Baseline
SR1
SR2
SR3
SR4
SR5
SR6
c
MAGT (°C)
-1.4
-1.6
-1.8
-2.0
1989
1999
2009
d
Permafrost loss (10^6 km^2)
0.06
0.03
0.00
-0.03
-0.06
e
Difference in ALT (m)
0.2
0.0
-0.2
-0.4
f
Difference in MAGT (°C)
0.2
0.0
-0.2
-0.4
SR1
SR2
SR3
SR4
SR5
SR6

Figure 3.

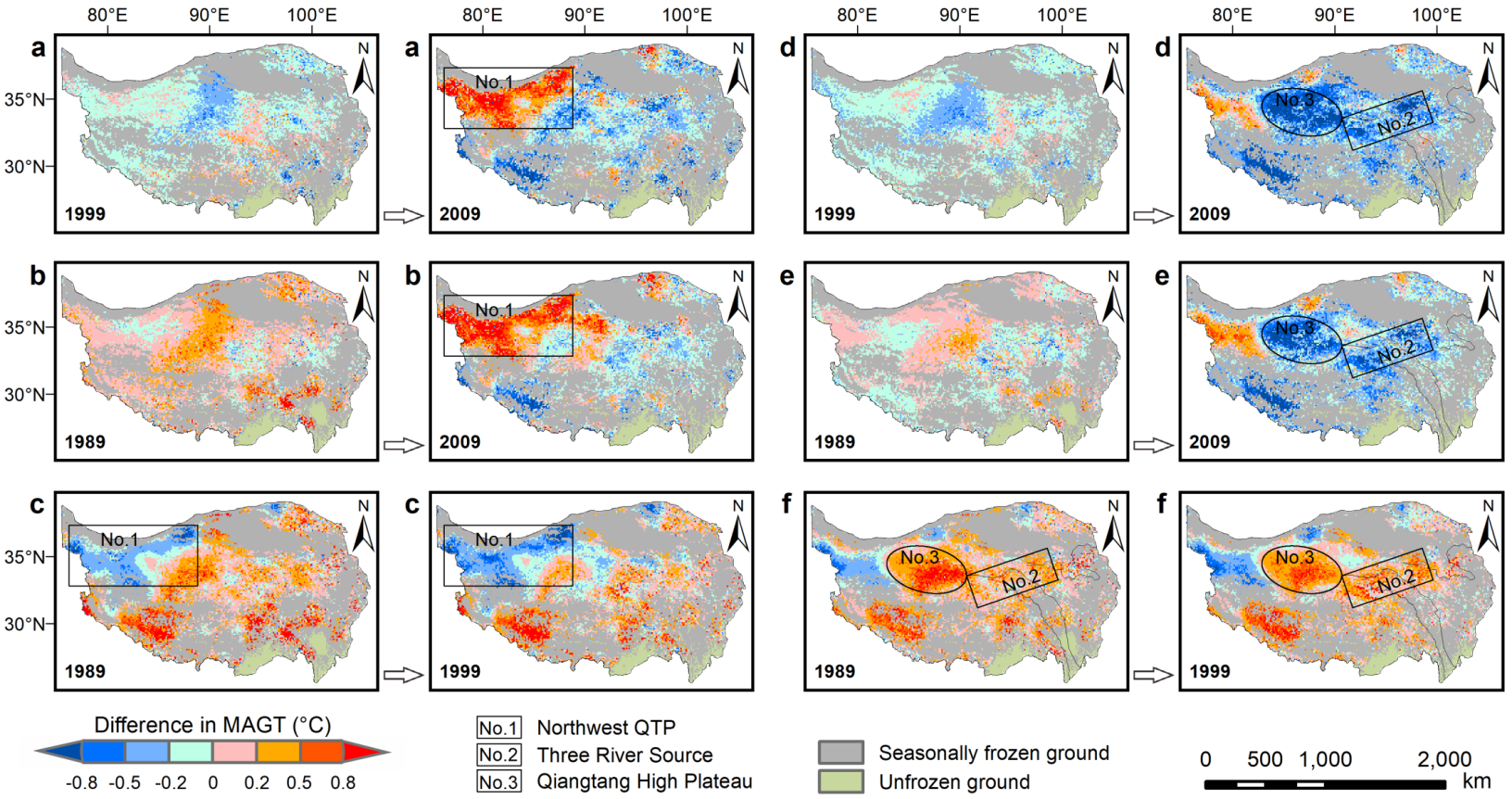
80°E
90°E
100°E
35°N
30°N
N
a
1999
a
2009
No.1
b
1989
b
2009
No.1
c
1989
c
1999
No.1
d
1999
d
2009
No.3
No.2
e
1989
e
2009
No.3
No.2
f
1989
f
1999
No.3
No.2
Difference in MAGT (°C)
-0.8 -0.5 -0.2 0 0.2 0.5 0.8
No.1 Northwest QTP
No.2 Three River Source
No.3 Qiangtang High Plateau
Seasonally frozen ground
Unfrozen ground
0 500 1,000 2,000
km

Figure 4.

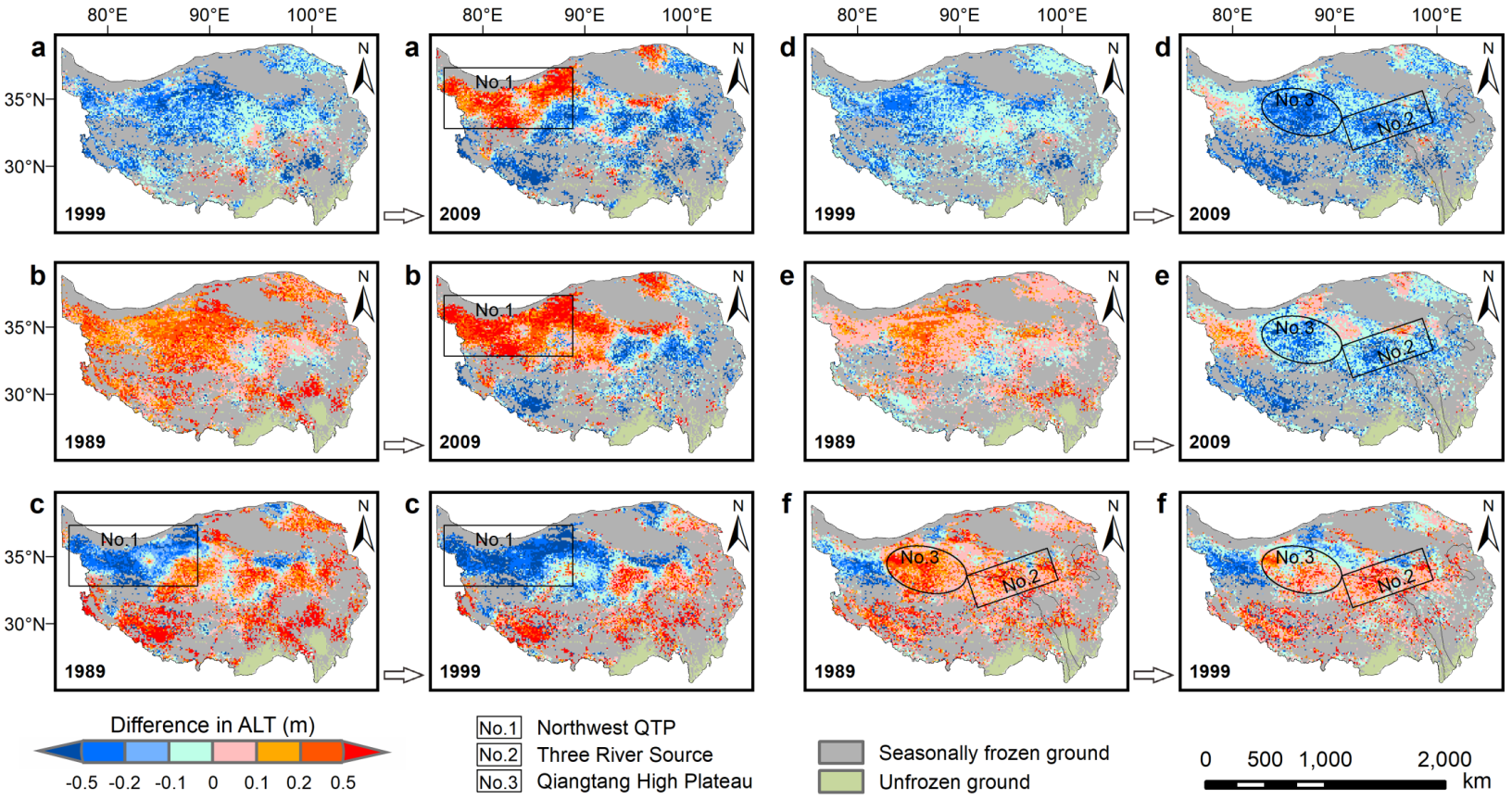
80°E
90°E
100°E
35°N
30°N
N
a
1999
a
2009
No.1
b
1989
b
2009
No.1
c
1989
c
1999
No.1
d
1999
d
2009
No.3
No.2
e
1989
e
2009
No.3
No.2
f
1989
f
1999
No.3
No.2
Difference in ALT (m)
-0.5 -0.2 -0.1 0 0.1 0.2 0.5
No.1 Northwest QTP
No.2 Three River Source
No.3 Qiangtang High Plateau
Seasonally frozen ground
Unfrozen ground
0 500 1,000 2,000
km

Figure 5.

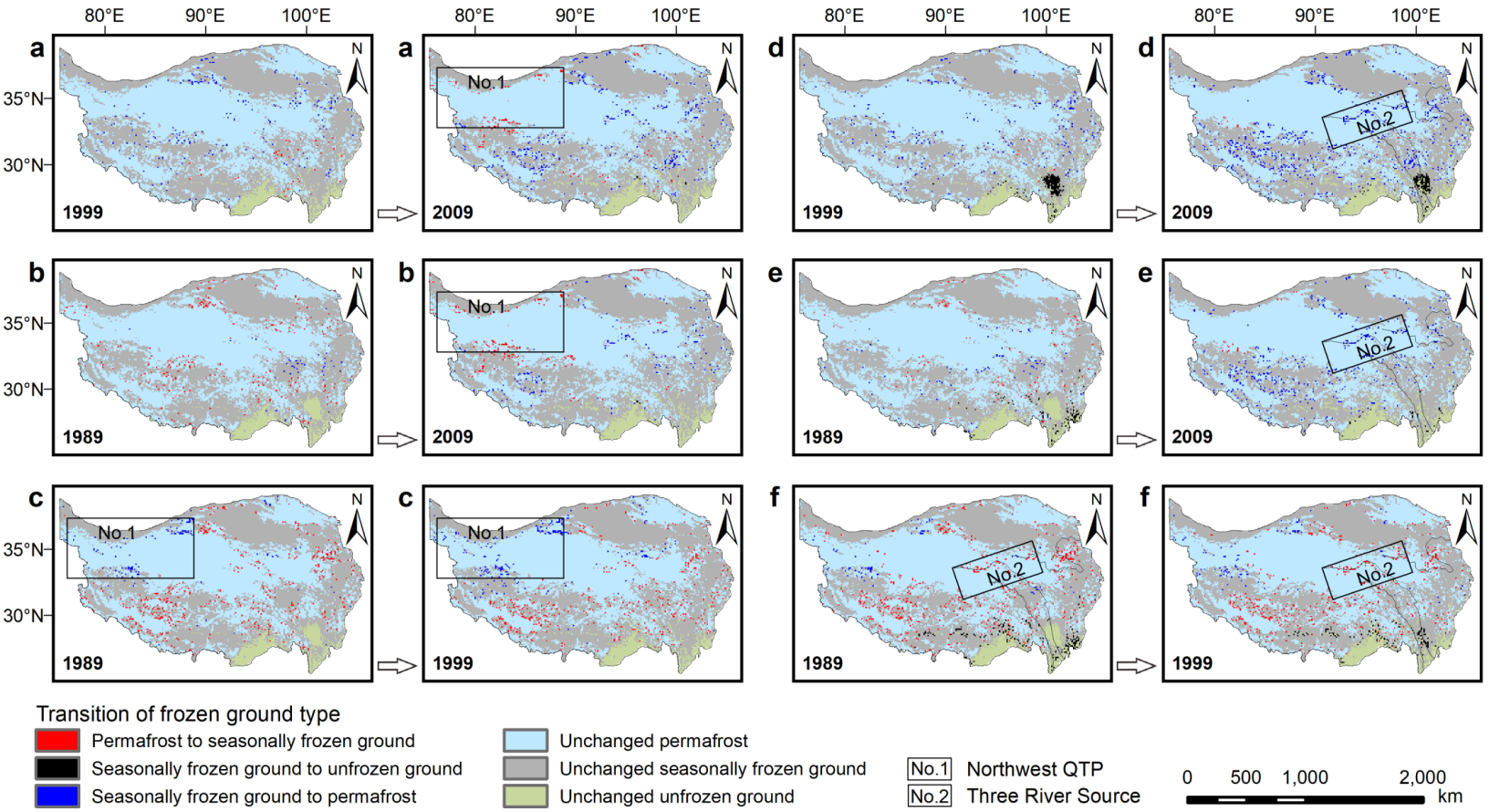
80°E
90°E
100°E
35°N
30°N
N
a
1999
a
2009
No.1
d
1999
d
2009
No.2
b
1989
b
2009
No.1
e
1989
e
2009
No.2
c
1989
c
1999
No.1
f
1989
f
1999
No.2
Transition of frozen ground type
Permafrost to seasonally frozen ground
Seasonally frozen ground to unfrozen ground
Seasonally frozen ground to permafrost
Unchanged permafrost
Unchanged seasonally frozen ground
Unchanged unfrozen ground
No.1 Northwest QTP
No.2 Three River Source
0 500 1,000 2,000
km